Radboud Repository

Radboud University Nijmegen

PDF hosted at the Radboud Repository of the Radboud University Nijmegen

This full text is a publisher's version.

For additional information about this publication click this link.
http://hdl.handle.net/2066/13810

Vibrational predissociation in the HCl dimer

G. W. M. Vissers, L. Oudejans, R. E. Miller, G. C. Groenenboom, and A. van der Avoird

Additional information on J. Chem. Phys.

Vibrational predissociation in the HCl dimer

G. W. M. Vissers
Institute of Theoretical Chemistry, NSRIM, University of Nijmegen, Toernooiveld 1, 6525 ED Nijmegen, The Netherlands

L. Oudejans[a)] and R. E. Miller
Department of Chemistry, University of North-Carolina, Chapel Hill, North Carolina 27599

G. C. Groenenboom and A. van der Avoird
Institute of Theoretical Chemistry, NSRIM, University of Nijmegen, Toernooiveld 1, 6525 ED Nijmegen, The Netherlands

We present results of a combined theoretical and experimental study on the vibrational predissociation of the HCl dimer. On the theoretical side, photodissociation linewidths and product-state distributions for monomer stretch excited states with total angular momentum $J=0$ were computed, using the Fermi golden rule approximation. The resonances investigated include excitation of the hydrogen bond donor and acceptor stretches, as well as combinations of one of these modes with the intermolecular stretch and geared bend modes, for both even and odd permutation symmetry. Line strengths for the transitions from the $J=1$, $K=0$ ground state to excited states with $J=0$ were computed using quasibound states. On the experimental side, the photofragment angular distribution method was employed to obtain complete final-state distributions for the monomer stretch excited states. Three different transitions were probed, all starting from the lower tunneling component of the ground state: the $^{R}Q_0(1)$ transition for excitation of the acceptor stretch and the $^{Q}R_0(0)$ transition and unresolved $^{R}Q_0$ branch for the donor stretch excitation. We find that, in contrast to the HF dimer, the excited-state alignment of the HCl dimer, resulting from excitation using a polarized laser beam, is completely lost on the time scale of the dissociation. The agreement between theory and experiment for the product-state distributions and line strengths is reasonable. The computed lifetimes are 1–2 orders of magnitude too small, which is attributed to a deficiency in the potential energy surface. © *2004 American Institute of Physics.* [DOI: 10.1063/1.1711601]

I. INTRODUCTION

Hydrogen bonding is one of the most important interactions in nature. It is studied in many areas of science, ranging from chemistry and physics to biology. For a quantitative description of such a bond, it is helpful to study small model systems. The simplest of these are hydrogen halide dimers, such as $(HF)_2$ and $(HCl)_2$. In the past few decades, considerable progress has been made in the description of these systems, both experimentally[1–10] and theoretically.[11–22]

Despite the obvious similarities between $(HF)_2$ and $(HCl)_2$, it is well known that their vibrational dynamics are quite different. For example, although both of these systems consist of a proton-acceptor–proton-donor pair, the HCl dimer has been shown both spectroscopically[1,3–5,9,23,24] and theoretically[11,12,14–16,25–27] to be much floppier than HF dimer. This is illustrated by the fact that the geared tunneling frequency in the ground state of the HF dimer is 0.66 cm^{-1},[6,7] while the corresponding value for the HCl dimer is as large as 15.5 cm^{-1}.[4,9] Since this value is comparable to the rotational energy spacing ($j=1\leftarrow 0$) in the monomer (21 cm^{-1}), it seems that the HCl molecules undergo nearly free

rotation in the dimer. This is consistent with the observation that the dissociation energy of the HCl dimer is much lower [439±1 cm^{-1} (Ref. 28)] than that of the HF dimer [1062±2 cm^{-1} (Ref. 29)].

This paper deals with the vibrational predissociation of the HCl dimer. Although there are a large number of papers on the vibrational predissociation of the HF dimer,[21,29–42] the corresponding data set for the HCl dimer is rather small. While there are a number of experimental studies that have been published,[28,43–48] theoretical efforts have been restricted to bound-state calculations of the vibration–rotation–tunneling levels of the HCl stretch excited dimer.[15] To our knowledge, no theoretical description of the photodissociation of monomer stretch excited $(HCl)_2$ has been published.

The dramatic difference in the tunneling rates for HF and HCl dimers is potentially of great significance with regard to the associated vibrational predissociation dynamics. In several previous publications[29,36,42] it was shown that the final HF-fragment rotational-state distribution resulting from vibrational predissociation of HF dimer can be understood in terms of the asymmetric equilibrium structure, which makes the proton donor and acceptor molecules in the parent complex quite different. In particular, the proton donor molecule receives a large torque as the molecules recoil, while the

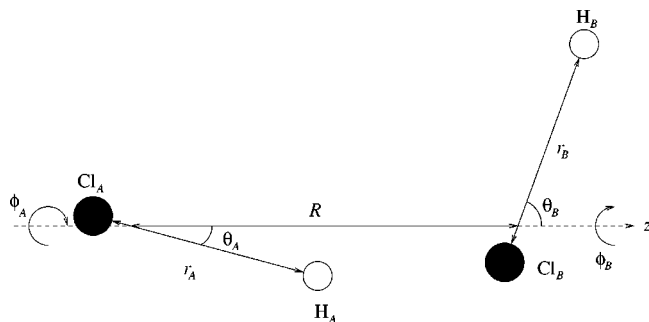a)Current address: Arcadis G&M, Inc., P.O. Box 13109, Research Triangle Park, NC 27709.

FIG. 1. Jacobi coordinates for the HCl dimer. The intermolecular vector **R** with length R connects the centers of mass of the two molecules and coincides with the z axis. θ_X, $X=A$, B, is the angle between molecule X and the z axis, ϕ_X the torsional angle. The intramolecular distances are denoted r_X.

force on the proton acceptor acts nearly through its center of mass. In view of the qualitatively different tunneling dynamics associated with the HCl dimer, we were interested in exploring the effects this has on the associated vibrational predissociation dynamics.

In this paper, we present the results of full-dimensional [six-dimensional (6D)] quantum calculations on the vibrational predissociation of the H ^{35}Cl dimer, for total angular momentum $J=0$. In a previous study on the vibrational predissociation of HF dimer it was shown that the Fermi golden rule approximation gives linewidths and product-state distributions that are in good agreement with full coupled channels calculations.[42] The same study also showed that the use of quasibound states to compute line strengths for the transitions to the vibrationally predissociating states is justified. We therefore applied the same approximations to the HCl dimer. We report lifetimes and rotational-state distributions for the hydrogen bond acceptor and donor stretch modes, as well as for combinations of these excitations with an in-plane geared bend and dimer stretch excitations. Furthermore, we report calculated line strengths for the corresponding transitions to these excited states. All calculations were performed for dissociation from states of both even and odd permutation symmetry.

We also present the results of an experimental study of HCl dimer vibrational predissociation. The photofragment angular distribution method, discussed previously for the HF dimer,[29] was used to obtain final-state distributions, including information on the intermolecular rotational-state correlations and recoil kinetic energy.

II. THEORY

The Hamiltonian for the system in the Jacobi coordinates (see Fig. 1) has been described previously in our paper on the HF dimer.[42] It consists of the sum of the two monomer Hamiltonians, a dimer kinetic energy term, and the interaction potential:

$$\hat{H}=\hat{h}_A+\hat{h}_B-\frac{\hbar^2}{2\mu R}\frac{\partial^2}{\partial R^2}R+\frac{\hat{J}^2+\hat{j}_{AB}^2-2\hat{\mathbf{j}}_{AB}\cdot\hat{\mathbf{J}}}{2\mu R^2}$$

$$+V_I(R,\mathbf{r}_A,\mathbf{r}_B),\qquad(1)$$

where $\hat{\mathbf{J}}$ is the total angular momentum of the dimer and $\hat{\mathbf{j}}_{AB}$ is the vector sum of the monomer angular momentum operators $\hat{\mathbf{j}}_A$ and $\hat{\mathbf{j}}_B$.

The bound-state wave functions are expanded in a body-fixed (BF) basis:

$$|nv_Av_B(j_Aj_B)j_{BA}K;JM\rangle$$

$$=|n\rangle|v_Aj_A\rangle|v_Bj_B\rangle|(j_Aj_B)j_{BA}K;JM\rangle,\qquad(2)$$

where $|n\rangle\equiv\varphi_n(R)$ is a dimer stretch basis function. The $|v_Xj_X\rangle\equiv\chi_{v_Xj_X}(r_X)$ are eigenfunctions of the monomer Hamiltonian $\hat{h}_X$ with eigenvalues $\epsilon_{v_Xj_X}$ and are obtained using a sinc function discrete variable representation (DVR).[49] The angular basis functions are given by

$$|(j_Aj_B)j_{AB}K;JM\rangle=\sqrt{\frac{2J+1}{4\pi}}D_{MK}^{(J)}(\alpha,\beta,0)^*$$

$$\times\sum_{m_Am_B}|j_Am_A\rangle|j_Bm_B\rangle$$

$$\times\langle j_Am_Aj_Bm_B|j_{AB}K\rangle,\qquad(3)$$

with $|j_Xm_X\rangle\equiv Y_{m_X}^{(j_X)}(\hat{\mathbf{r}}_X)$ spherical harmonics, coupled by a Clebsch–Gordan coefficient $\langle j_Am_Aj_Bm_B|j_{AB}K\rangle$. The Wigner rotation function $D_{MK}^{(J)}(\alpha,\beta,0)^*$ depends on the polar angles (β,α) of the intermolecular vector **R** with respect to a space-fixed frame.

The dimer stretch basis functions are given by $\varphi_n(R)=\tilde{\varphi}_n(R)/R$, where the $\tilde{\varphi}_n(R)$ are eigenfunctions of a reference Hamiltonian

$$\hat{h}^{\text{ref}}=-\frac{\hbar^2}{2\mu}\frac{\partial^2}{\partial R^2}+V^{\text{ref}}(R).\qquad(4)$$

The reference potential $V^{\text{ref}}(R)$ is obtained by minimizing the full 6D potential in all coordinates but R. The eigenfunctions of $\hat{h}^{\text{ref}}$ are also computed using a sinc function DVR.

The angular part of the interaction potential is expanded in functions of the type of Eq. (3), with expansion coefficients depending on r_A, r_B, and R. Since the potential is invariant under overall rotations of the system, it does not depend on α and β or on ϕ_A and ϕ_B separately, but only on the difference angle $\phi=\phi_B-\phi_A$. Hence only the terms with $J=K=0$ appear in the expansion, so that the expansion functions for the potential can be written

$$A_{L_AL_BL}=(-1)^{L_A+L_B+L}$$

$$\times\sum_{M_A}\begin{pmatrix}L_A & L_B & L\\ M_A & -M_A & 0\end{pmatrix}|L_AM_A\rangle|L_B-M_A\rangle.$$

$$(5)$$

In our work on the infrared photodissociation of the HF dimer, we found that the Fermi golden rule approximation gives lifetimes and rotational-state distributions which are in good agreement with a full coupled channels calculation.[50] We will therefore apply this approximation also to the HCl–HCl system. In the golden rule approximation, the linewidth Γ of a resonance is given by

J. Chem. Phys., Vol. 120, No. 20, 22 May 2004

Predissociation in the HCl dimer   9489

$$\Gamma = \sum_{j_A j_B} \Gamma_{j_A j_B} = \sum_{j_A j_B j_{AB} lM} \frac{2\pi}{\hbar} |\langle \psi_b | V_{10} | \psi_{JM}^{(-)j_A j_B j_{AB} l} \rangle|^2,$$

(6)

where the V_{10} is the vibrational coupling potential between HCl-stretch excited- $(v_A + v_B = 1)$ and ground- $(v_A = v_B = 0)$ state basis functions. The bound state $|\psi_b\rangle$ is calculated in a basis without the ground-state functions, and $\psi_{JM}^{(-)j_A j_B j_{AB} l}$ is the energy normalized scattering wave function calculated in a basis with ground-state HCl-stretch functions only. The rotational-state distribution can be defined as the ratio of the partial linewidths to the total linewidth:

$$P_{j_A j_B} = \frac{\Gamma_{j_A j_B}}{\Gamma}.$$

(7)

As in our work on the photodissociation of the HF dimer,[42] the scattering wave function $\psi_{JM}^{(-)j_A j_B j_{AB} l}$ is expanded in a space-fixed basis $|(j_A j_B)j_{AB} l;JM\rangle^{SF}$, which is related to the body-fixed basis via a unitary transformation:

$$|(j_A j_B)j_{AB} l;JM\rangle^{SF}$$
$$= \sum_K |(j_A j_B)j_{AB} K;JM\rangle \sqrt{\frac{2l+1}{2J+1}} \langle j_{AB} K; l0|JK\rangle.$$

(8)

Using the expansion

$$\psi_{JM}^{(-)j_A j_B j_{AB} l}(\mathbf{R}, \mathbf{r}_A, \mathbf{r}_B) = \sum_{v_A' v_B' j_A' j_B' j_{AB}' l'} R^{-1} f_{v_A' v_B' j_A' j_B' j_{AB}' l'}^{j_A j_B j_{AB} l}(R)$$
$$\times |(j_A' j_B')j_{AB}' l';JM\rangle^{SF},$$

(9)

the expansion coefficients $f_{v_A' v_B' j_A' j_B' j_{AB}' l'}^{j_A j_B j_{AB} l}(R)$ can for large R be written as

$$f_{v_A' v_B' j_A' j_B' j_{AB}' l'}^{j_A j_B j_{AB} l}(R)$$

$$= \frac{1}{\sqrt{2\pi\hbar}} [v_{v_A' v_B' j_A' j_B' l'}(R) \delta_{v_A' 0} \delta_{v_B' 0} \delta_{j_A' j_A} \delta_{j_B' j_B} \delta_{j_{AB}' j_{AB}} \delta_{l' l}$$

$$- u_{v_A' v_B' j_A' j_B' l'}(R) S^*_{v_A' v_B' j_A' j_B' l', 00 j_A j_B l}],$$

(10)

where $\mathbf{S}$ is the scattering matrix.[51] The flux normalized outgoing waves $v_{v_A v_B j_A j_B l}(R)$ and incoming waves $u_{v_A v_B j_A j_B l}(R)$ are given by

$$v_{v_A v_B j_A j_B l}(R) = i \sqrt{\frac{\mu k_{v_A v_B j_A j_B}}{\hbar}} R h_l^{(1)}(k_{v_A v_B j_A j_B} R),$$ (11)

$$u_{v_A v_B j_A j_B l}(R) = -i \sqrt{\frac{\mu k_{v_A v_B j_A j_B}}{\hbar}} R h_l^{(2)}(k_{v_A v_B j_A j_B} R)$$

$$= v_{v_A v_B j_A j_B l}(R)^*,$$

(12)

where $h_l^{(1)}$ and $h_l^{(2)}$ are spherical Hankel functions of the first and second kind,[52] respectively, and where the wave numbers $k_{v_A v_B j_A j_B}$ are defined as

$$k_{v_A v_B j_A j_B} = \sqrt{\frac{2\mu(E - \epsilon_{v_A j_A} - \epsilon_{v_B j_B})}{\hbar^2}}.$$

(13)

TABLE I. Overview of dissociation energy and tunneling splittings, in cm^{-1}, computed on the ES1 and ES1–EL potentials. $\Delta(\nu)$ denotes the tunneling splitting in state ν. The ground state is denoted ν_0 here; ν_1 and ν_2 refer to the acceptor and donor stretch excited states.

	ES1	ES1–EL	Expt.
D_e	693.71	694.12	
D_0	416.25[a]	425.25	439[b]
$\Delta(\nu_0)$	14.94[a]	15.22	15.47668[c]
$\Delta(\nu_1)$	0.03[d]	−2.31	−3.3237[e]
$\Delta(\nu_2)$	−0.04[d]	2.46	3.1760[e]

[a]Reference 15.
[b]Reference 28.
[c]Reference 4.
[d]Reference 16.
[e]Reference 44.

III. COMPUTATIONAL DETAILS

The ES1–EL (Ref. 16) potential energy surface was used in the present calculation. This potential surface is based on the earlier ES1 potential[14] by Elrod and Saykally. The ES1 potential is a fit to a large amount of spectroscopic data, with an earlier *ab initio* potential by Bunker *et al.*[12] as a starting point. However, this fit used four-dimensional calculations (i.e., excluding the monomer vibrations) to modify only some of the intermolecular parameters, while leaving the intramolecular parameters untouched. In the *ab initio* potential and, consequently, also in the ES1 potential, the dependence on the monomer stretch coordinates was found to be much too weak. This problem was partially solved in an *ad hoc* manner by Qiu *et al.* with the addition of an electrostatic interaction potential, leading to the ES1–EL potential.[16] This relatively simple modification gave tunneling splittings in the monomer stretch excited state that were in much better agreement with experiment (see Table I for a number of relevant parameters). We expanded this potential in terms of angular functions of Eq. (5) up to $L_A, L_B = 13$.

The quasibound-state wave functions and energies have been calculated in a basis with $j_A, j_B \leq 13$, $v_A + v_B \leq 2$, and $n \leq 8$, giving a basis of approximately 28 500 functions. This was found to be sufficient to converge the energies to within 0.01 cm^{-1}. The monomer eigenfunctions were calculated using a sinc function DVR on an equally spaced grid of 35 points in the range $(1.6-3.7)a_0$. For the dimer stretch basis functions, an equally spaced grid of 185 points between $6a_0$ and $11a_0$ was used. To compute the monomer stretch excited states, a three-step diagonalization of the Hamiltonian was used, which is described in our paper on the bound states of the HF dimer.[50]

The bound state $|\psi_b\rangle$ in the golden rule expression was calculated in a basis with $v_A + v_B = 1$, 2, $j_A, j_B \leq 13$, and $n \leq 8$. The radial scattering wave function was represented on an equally spaced 332-point grid, in the range $(3-21)a_0$. A renormalized Numerov[53] propagator was used to compute this wave function. The radial integral was built up in parallel to the propagation, using a method similar to that described by Gadéa *et al.*[54] In the propagation, the scattering wave function was represented in the body-fixed basis; the transformation to the space-fixed basis was not performed until the matching of the wave function to the asymptotic

solutions. Rotational channels up to $j_A, j_B \leq 16$ were used to describe the scattering wave function, giving a total of ≈ 800 dissociation channels for scattering states of odd exchange symmetry and ≈ 1000 channels for the even states. About half of the available channels were open in the investigated energy range, up to $(j_A, j_B) = (2,15)$ for the resonance highest in energy $(\nu_1 + \nu_5)$.

In the calculation of the line strengths of the transitions, the dimer dipole moment was approximated by the sum of the vibrational transition dipole moments of the monomers, $\langle 1|\hat{\mu}_{HCl}|0\rangle$. The same approximation was used for the HF dimer,[42] and matrix elements for the dimer transition dipole in the basis of Eq. (2) are given there.

IV. EXPERIMENTAL METHOD

The experimental method used in this study has been discussed in detail elsewhere.[29] The apparatus consists of a rotatable molecular beam source that is collimated by two skimmers to provide high angular resolution. The HCl dimer was formed by expanding a 5% mixture of HCl in helium through a (room-temperature) 50-μm-diam nozzle from a source pressure of 600 kPa. In addition, a mix with 20% of the amount of helium replaced by argon was used to reduce the beam velocity, enhancing the angular resolution. Since the near-infrared spectrum of the HCl dimer is well known from previous studies,[1,9,44,46] no searching for the transitions of interest was required. The main experimental challenge in the present study was getting the F-center laser, used to excite the dimer to the vibrationally excited state, to operate at long enough wavelengths to reach the two HCl stretching vibrations. This required using a grating with a lower output efficiency to extend the tuning range of the laser. In combination with a new crystal in the laser, this change provided usable single-mode output powers out to 2825 cm^{-1}, sufficient to reach all of the HCl dimer bands, including the ν_1 and ν_2 vibrations.

The spectra were first recorded by positioning the bolometer detector 5° off the beam axis to detect the fragments resulting from the vibrational predissociation of the dimer. A spherical multipass cell[29] was used to obtain approximately 60 passes of the laser through the molecular beam, within a small focal volume approximately 1.5 mm on a side. Tuning of the laser was computer controlled and several evacuated confocal étalons and a wavemeter were used for frequency calibration and monitoring of the tuning. Once the transition of interest was found, the laser was tuned to the top of the peak, locked to a 150-MHz étalon fringe, and the angular distribution was recorded by integrating the signal for 10 s at the observation angles, separated by 0.25°. For details of the relationship between these angular distributions and the kinetic energy release and, thus, of the internal-state distribution of the fragments, the reader is referred to previous publications.[33,35] In the analysis of the experimental data, a Monte Carlo method was used to account for all of the instrumental factors that contribute to the shape of the angular distributions.

Since the relationship between the scattering angle in the laboratory frame and the recoil energy depends directly upon the velocity of the parent molecule, it is essential that we

TABLE II. Quasibound state energies of the HCl dimer, in cm^{-1}. All resonance frequencies are relative to the ground state.

	A_1		B_2	
	Calc.	Expt.	Calc.	Expt.
ν_1	2876.69	2883.5732[a]	2874.38	2880.2495[a]
$\nu_1 + \nu_4$	2942.53		2940.65	
$\nu_1 + \nu_5$	2967.23		2964.93	
ν_2	2857.01	2854.0593[a]	2859.47	2857.23528[a]
$\nu_2 + \nu_4$	2931.99	2930.84331[b]	2933.92	
$\nu_2 + \nu_5$	2912.57		2915.15	2915.98595[c]

[a]Reference 44.
[b]References 4 and 47.
[c]Reference 47.

have an accurate measurement of the latter. In the present study we made use of Doppler spectroscopy to accurately determine both the velocity and velocity distribution of the HCl dimer in the molecular beam. The result of this measurement was a velocity for the 5% HCl in a He mixture of 1465 and 995 m/s for the (20% argon)/(5% HCl) in the helium mixture. These values are in good agreement with those estimated from the percentage weighted mass of the expanding gas: namely, 1480 and 980 m/s, respectively.

V. RESULTS

A. Calculations

The monomer stretch excitations are labeled ν_1 for excitation of the hydrogen bond acceptor (the "free" HCl molecule) and ν_2 for excitation of the donor (the "bound" molecule). The intermolecular modes are ν_4 for excitation of the dimer stretch and ν_5 for the in-plane geared bend. The calculations were performed for ν_1, $\nu_1 + \nu_4$, $\nu_1 + \nu_5$, ν_2, $\nu_2 + \nu_4$, and $\nu_2 + \nu_5$ modes, for total angular momentum $J = 0$ and for both even (A_1) and odd (B_2) states with respect to monomer exchange. The computed predissociating states are all even with respect to spatial inversion. Following normal conventions in IR spectroscopy, we will also label transitions to excited states of B_2 symmetry with ν^+ and transitions to states of A_1 symmetry with ν^-. The calculated energies of the quasibound states studied in this paper are given in Table II, together with the available experimental frequencies. The calculated values given here are nearly identical to those reported by Qiu *et al.*[16] using the same potential energy surface (PES).

The theoretical linewidths, computed at the quasibound-state energies, are given in Table III. Comparison with the experimental linewidths shows that the theoretical values with the ES1–EL potential are 1–2 orders of magnitude too small. A problem in the calculation of the linewidths is the strong dependence of the linewidth on the total energy at which the golden rule calculation is performed. An extreme example of this can be seen in Fig. 2, where the linewidth for the ν_1^- excitation is plotted for a range of energies around the quasibound energy. Not all vibrational resonances exhibit the same Lorentzian variation in linewidth as this ν_1 resonance, but it serves to show that a small shift in total energy can dramatically change the theoretical linewidth. This is most

TABLE III. Vibrational predissociation linewidths Γ, in MHz. The experimental linewidths reported for Ref. 28 have been calculated from the lifetimes which were measured directly in a time resolved, pulsed laser experiment.

	A_1		B_2	
	Calc.	Expt.	Calc.	Expt.
ν_1	0.1074	3.5 ± 0.4[a]	0.0844	<1.6[b]
$\nu_1 + \nu_4$	0.0473		0.1616	
$\nu_1 + \nu_5$	0.0290		0.1996	
ν_2	0.0366	5.7 ± 0.2[a]	0.0225	5.1 ± 1.2,[b] 8.4 ± 1.6[a]
$\nu_2 + \nu_4$	0.1516	9 ± 3[c]	0.0616	
$\nu_2 + \nu_5$	0.0574		0.0189	3 ± 3[c]

[a]Reference 28.
[b]Reference 44.
[c]Reference 47.

likely due to a rotational resonance, an effect that was observed previously in the vibrational predissociation of the Ar–CH$_4$ complex.[55] However, we were unable to analyze this resonance due to the large number of rotational channels involved. Note that for this resonance, the discrepancy with experiment is even worse if the golden rule calculation is done at a different energy.

The rotational-state distributions of the fragments are much less dependent on the energy at which the computation is performed. Whereas the linewidth can change dramatically over a range of $1–2$ cm^{-1}, these distributions remain fairly constant over the same range. Therefore it is safe to discuss particular features found in these distributions. We will label the dissociation channels with a pair of rotational quantum numbers (j_1, j_2), which denotes a symmetrized combination of basis functions with $(j_A, j_B) = (j_1, j_2)$ and $(j_A, j_B) = (j_2, j_1)$.

Figure 3 shows the rotational-state distributions (j_1, j_2) for the ν_2 and ν_1 scattering states of A_1 symmetry. An overview of the most important contributions to the rotational-state distributions for all the resonances investigated is given in Tables IV and V. The most striking feature is the high

FIG. 3. Calculated rotational-state distribution for the (a) ν_2 and (b) ν_1 excited states of A_1 symmetry. The dashed line indicates the total amount of kinetic energy available. The most important channels are marked with their product rotational quantum numbers (j_1, j_2).
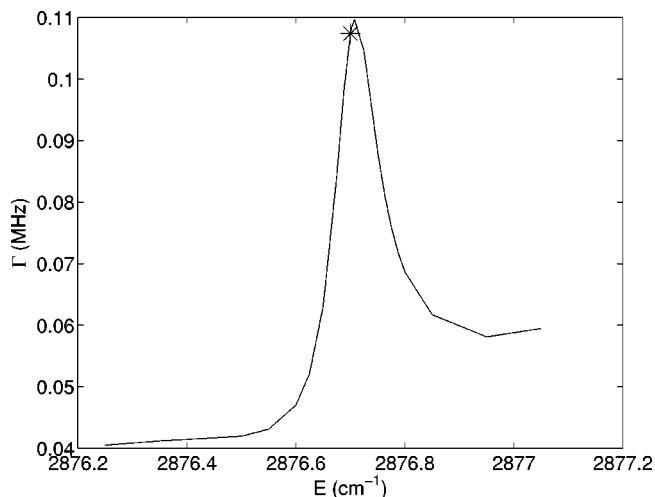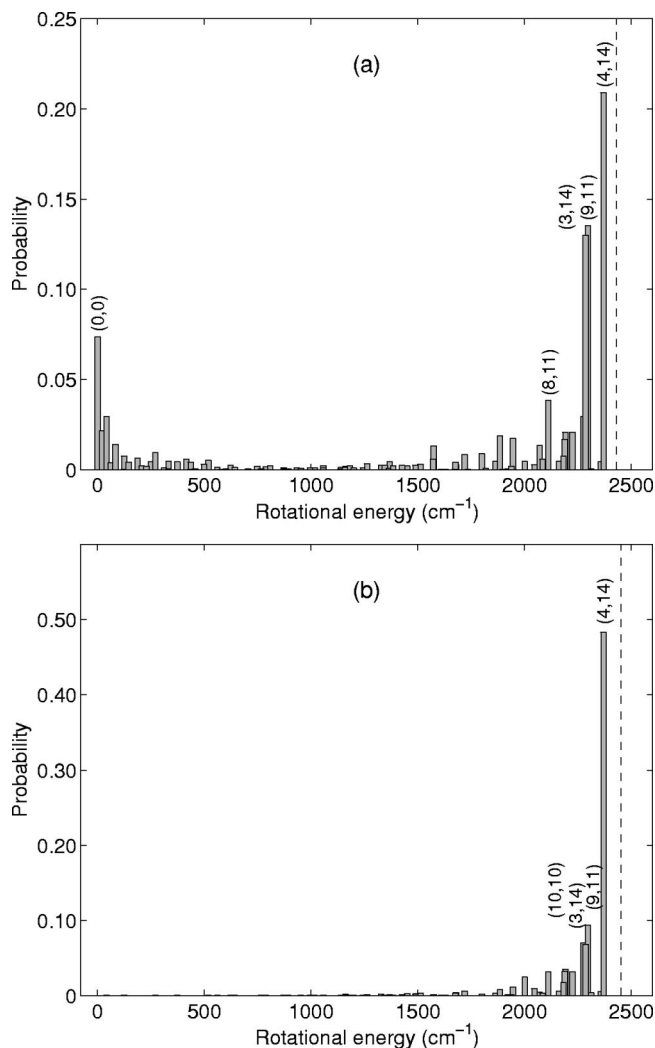
FIG. 2. Fermi golden rule linewidth of the ν_1 excited state of A_1 symmetry as a function of the energy at which the calculation is performed. The star indicates the line width at the energy of the quasibound state.

contribution of the lower rotational channels to the distribution of the ν_2 excited state. This is in stark contrast with the ν_1 resonance of the same symmetry, where the contribution from these product channels is negligible. Instead, nearly all photofragments end up in the higher rotational channels for this resonance, with nearly half of them in the highest open channel: namely, (4,14).

Inspection of the distributions for the other states shows that there are more excitations for which the contribution of the lower rotational channels is significant. These are the $(\nu_2 + \nu_4)^-$ and $(\nu_2 + \nu_5)^-$ resonances and, to a lesser extent, the $(\nu_1 + \nu_4)^+$ and the $(\nu_2 + \nu_4)^+$ resonances. In comparison, the larger anisotropy associated with the HF dimer[42] results in all HF fragments being produced in highly rotationally excited channels. This is consistent with earlier studies, which show that not only is the HCl–HCl hydrogen bond weaker than that in the HF dimer, it is also less directional.

Using a quasibound-state approximation to the excited states, we computed the line strengths for transitions from the $J=1$, $K=0$ ground state to the $J=0$ predissociating states, as summarized in Table VI. The symmetry labels in

TABLE IV. Overview of the most important contributions (highest probabilities) to the rotational state distributions, for scattering states of A_1 symmetry. The last two lines show the distribution of the excess energy, in cm^{-1}, over rotational and translation energy of the fragments. All values are percentages.

(j_A, j_B)	ν_1^-	$(\nu_1 + \nu_4)^-$	$(\nu_1 + \nu_5)^-$	ν_2^-	$(\nu_2 + \nu_4)^-$	$(\nu_2 + \nu_5)^-$
(0,0)	0.02	0.01	0.17	7.37	1.28	1.62
(8,11)	3.18	6.66	1.60	3.84	2.88	4.18
(2,14)	3.17	2.73	0.49	2.08	0.16	5.47
(10,10)	7.03	1.52	0.26	2.94	2.16	2.94
(3,14)	6.82	6.10	1.98	13.00	3.40	4.45
(9,11)	9.39	7.11	1.57	13.52	15.32	16.08
(4,14)	48.36	12.78	8.18	20.90	8.46	8.33
(5,14)	0.00	12.02	22.47	0.00	17.81	11.86
(1,15)	0.00	5.03	9.49	0.00	1.82	0.00
(10,11)	0.00	23.63	17.24	0.00	24.36	0.00
(2,15)	0.00	0.00	14.70	0.00	0.00	0.00
E_{rot}	91.30	88.94	92.48	70.76	88.02	74.29
E_{trans}	8.70	11.06	7.52	29.24	11.98	25.71

the table refer to the symmetry of the excited states. Selection rules imply that only transitions from the upper tunneling level of the $J = 1$, $K = 0$ ground state (having A_2 symmetry) to the A_1 excited states and from the lower ground-state tunneling level (of B_1 symmetry) to the B_2 excited states are allowed.

B. Experiments

1. Acceptor stretch ν_1

From the previous infrared study of the HCl dimer[44] we know that the highest-frequency vibrational band with high intensity is located at 2890 cm^{-1}, corresponding to the $K_a = 1 \leftarrow 0$ subband of the ν_1 vibration, starting from the lower tunneling state. The dominant features in this spectral region are the three Q branches associated with the three dimer isotopic modifications: namely, $(H^{35}Cl)_2$, $H^{35}Cl–H^{37}Cl$, and $(H^{37}Cl)_2$. From earlier studies on the HF dimer[35] we know that the best possible resolution of the individual fragment states is found when the $^R R_0(0)$ transition is excited with the laser polarization direction parallel to the velocity vector of the parent molecule, assuming that the complex dissociates along its A axis. This is a result of the fact that this polarization selectively excites those molecules with their transition moments (approximately perpendicular to

their A axis) aligned parallel to the molecular beam direction. As a result, the fragments tend to scatter primarily to the maximum possible scattering angle and do not contribute to the signal at smaller angles, where the lower recoil energy fragments appear. Figure 4(a) shows the resulting angular distribution with parallel polarization. Although individual rotational channels are more closely spaced in angle than for HF dimer, owing to the larger mass of the HCl fragments, there is still some structure in the angular distribution, with clear evidence for at least three separate channels.

Before discussing the fitting of this angular distribution, it is helpful to consider the case when the polarization is directed perpendicular to the parent molecule velocity vector—i.e., perpendicular to the molecular beam. This angular distribution is shown in Fig. 4(b) and within the experimental uncertainties is identical to that obtained with parallel polarization. This is in stark contrast to the HF dimer[29] and other systems we have studied,[56,57] where the perpendicular polarization gives an angular distribution that is much more forward peaked, since now we selectively excite the parent molecules that are aligned with their transition moments perpendicular to the beam axis, which in the axial recoil limit would tend to give fragments that recoil near zero degrees. One obvious explanation for this would be that the system does not dissociate axially. However, before we can draw

TABLE V. As Table IV, for scattering states of B_2 symmetry.

(j_A, j_B)	ν_1^+	$(\nu_1 + \nu_4)^+$	$(\nu_1 + \nu_5)^+$	ν_2^+	$(\nu_2 + \nu_4)^+$	$(\nu_2 + \nu_5)^+$
(5,13)	6.42	5.51	0.14	1.90	2.90	0.77
(3,14)	6.24	2.99	0.91	6.82	0.84	6.00
(9,11)	13.25	6.91	0.56	4.82	3.95	1.98
(6,13)	7.08	2.93	2.19	11.54	2.49	2.47
(8,12)	27.61	17.93	2.11	27.38	13.24	15.75
(4,14)	21.74	7.73	3.24	27.49	4.21	11.84
(7,13)	0.00	6.26	17.86	0.00	12.20	14.78
(5,14)	0.00	11.03	42.17	0.00	25.69	27.54
(1,15)	0.00	6.69	1.43	0.00	0.66	0.11
(10,11)	0.00	11.99	12.13	0.00	10.86	0.00
(2,15)	0.00	0.00	12.45	0.00	0.00	0.00
E_{rot}	90.63	88.98	95.40	88.94	86.08	89.69
E_{trans}	9.37	11.02	4.60	11.06	13.91	10.31

TABLE VI. Line strengths from quasibound-state calculations in units of $|\langle 1|\hat{\mu}_{HCl}|0\rangle|^2$, where $\langle 1|\hat{\mu}_{HCl}|0\rangle$ is the monomer vibrational transition dipole moment. The transitions originate from the two tunneling levels of the $J=1$, $K=0$ ground state: $(J,K,\Gamma)=(1,0,A_2)\rightarrow(0,0,A_1)$ and $(1,0,B_1)\rightarrow(0,0,B_2)$.

	A_1	B_2
ν_1	0.5116	0.5649
$\nu_1+\nu_4$	0.0058	0.0014
$\nu_1+\nu_5$	0.0126	0.0032
ν_2	0.1398	0.2838
$\nu_2+\nu_4$	0.0543	0.0050
$\nu_2+\nu_5$	0.1863	0.0077

such a conclusion we need to consider the possibility that the alignment that is initially imposed on the system by excitation with a linearly polarized laser is lost before the molecule dissociates. There are two reasons we might expect such behavior. First, as already documented in the literature,[44] the predissociation lifetimes of the HCl dimer are considerably longer than those of HF dimer, giving the system more time to lose this alignment. In addition, the nuclear hyperfine
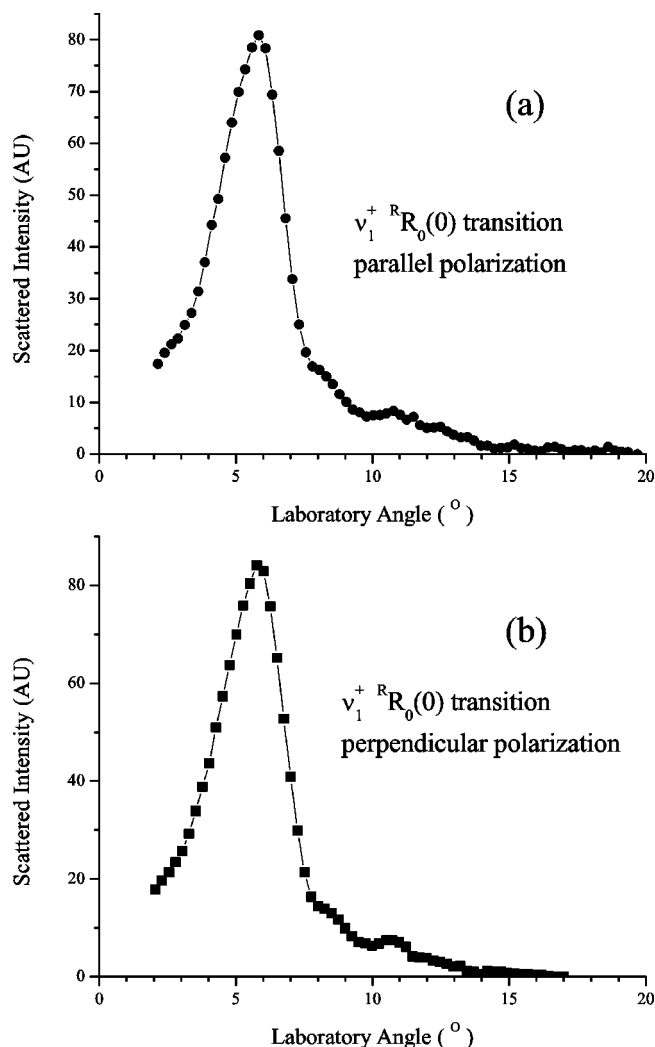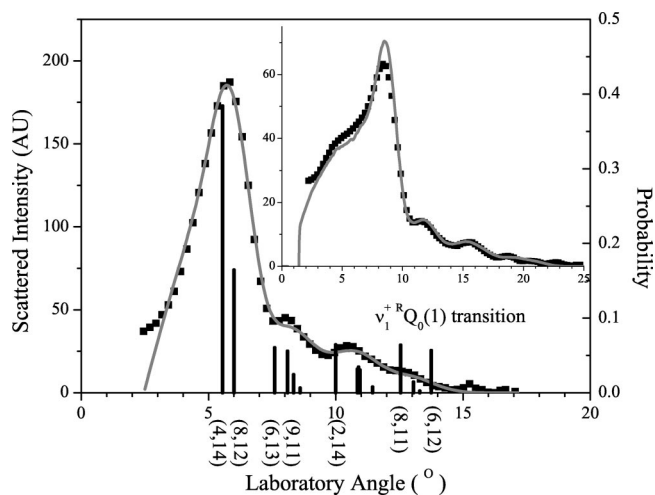

FIG. 5. Photofragment angular distribution for the ν_1^+ $^RQ_0(1)$ transition of the H^{35}Cl dimer. The solid line through the data points is the result of a Monte Carlo calculation over all the experimental parameters. The quantum number assignment (j_1,j_2) for the most important channels is denoted under the vertical bars indicating the probability for each channel. The inset shows the same angular distribution, but now for slower-molecular-stream-velocity conditions by using argon seeding of the molecular beam. The fragments scatter to larger laboratory angles than in a faster helium-seeded expansion.

splitting is very large in HCl, as indicated above, such that the nuclear hyperfine depolarization should be much faster than in HF dimer. In our earlier estimate for HF dimer we determined that the lifetime was much shorter than the depolarization time (by 4 orders of magnitude). For the HCl dimer, however, we estimate that the lifetime is approximately equal to the depolarization time, based on the electric quadrupole coupling constant of the chlorine: namely, approximately 68 MHz (Refs. 58 and 59) and a lifetime of the ν_1 HCl dimer of approximately 100 ns (linewidth: 1.6 MHz).[44]

A further test that the detailed shape of the angular distributions is independent of the initial alignment imposed by the excitation process comes from recording the angular distribution while having the laser tuned to the center of the largest peak in the Q branch. This angular distribution, shown in Fig. 5, is identical to the other two within the experimental uncertainty. As a result of these measurements, we conclude that the alignment is completely lost on the time scale for dissociation of the complex, which means that we cannot use the polarization method to determine whether or not the molecule dissociates in an axial fashion. In view of this, all the fits to the experimental angular distributions were carried out using an anisotropy parameter $\beta=0$.

The next step would be to obtain an angular distribution for the upper tunneling state of the ν_1 stretch. Unfortunately, the large tunneling splitting in the vibrational ground state (15.5 cm^{-1}), combined with the low rotational temperature of the molecular beam, made the signals for this state too low for detailed analysis.

As mentioned above, the heavy mass of the HCl fragment restricts the angular distributions to angles smaller than 17°. In an attempt to improve the angular resolution we also recorded angular distributions for the ν_1^+ $^RQ_0(1)$ transition

FIG. 4. Photofragment angular distributions of the ν_1^+ $^RR_0(0)$ transition resulting from photodissociation of the H^{35}Cl dimer for (a) parallel and (b) perpendicular laser polarization configurations.

using a gas mixture containing 20% argon. The lower velocity of the resulting molecular beam spreads out the angular distribution to 25°, as shown in the inset in Fig. 5.

The angular distributions obtained for the other two isotopic forms of the dimer were indistinguishable from those shown above. As a result, we present here only an analysis of the H^{35}Cl dimer. It is interesting to note, however, that the situation is quite different for the HF–HCl complex,[57,60] where both the lifetimes and final-state distributions are dependent upon the chlorine isotope.

2. Donor stretch ν_2

The "bound" HCl stretch is further redshifted from the HCl monomer, which makes it even more difficult to reach with the F-center laser. Nevertheless, we were successful in getting the laser to operate single mode at the appropriate frequency to observe the unresolved Q branch belonging to the $K_a = 1 \leftarrow 0$ subband at 2868.15 cm^{-1} as well as the $K_a = 0 \leftarrow 0$ subband transitions at 2857 cm^{-1}. This provides us with a unique opportunity to observe possible differences in the dynamics of the photodissociation upon excitation of an additional K_a quantum, within the same vibrational band.

Figure 6(a) shows an angular distribution obtained with the laser tuned to the top of the unresolved Q branch in the $K_a = 1 \leftarrow 0$ while in Fig. 6(b) the angular distribution for the $R(0)$, $K_a = 0 \leftarrow 0$ transition is shown. The angular distributions recorded in this way show no dependence on polarization direction, indicating once again that hyperfine depolarization is fast with respect to the dissociation lifetime. Again, we find that the angular distribution for all of the other isotopomers of the dimer in the $K_a = 0 \leftarrow 0$ subband are the same within the experimental uncertainty. Overall, the angular distribution is quite similar to that obtained from excitation of the "free" HCl stretch. However, due to the somewhat smaller excitation energy associated with the "bound" stretch, in comparison with the "free" stretch, the first peak in the angular distribution of the former appears at somewhat smaller angles than for the latter. Once again, transitions starting from the upper tunneling state were too weak for detailed analysis.

VI. DISCUSSION

A. Analysis of the angular distributions

Before discussing the assignment of the features in the angular distributions presented above, it is important to consider what is already known about the dissociation of the HCl dimer. First, the study of Pine and Howard[2] provides a reasonable estimate of the dissociation energy (D_0) of this complex: namely, 431 ± 22 cm^{-1}. This is extremely helpful since it defines, at least approximately, which channels are available. More recently, Ni *et al.*[28] obtained a more accurate value of $D_0 = 439 \pm 1$ cm^{-1}. Figure 7 shows an energy level diagram for the HCl dimer, using this value for the dissociation energy. It is interesting to note the rather large energy gap between the available energy and the first open channel. This is clearly consistent with the fact that the first peak in the experimental angular distributions appears at 5.8° following excitation of the "free" ν_1 HCl stretch, corresponding to
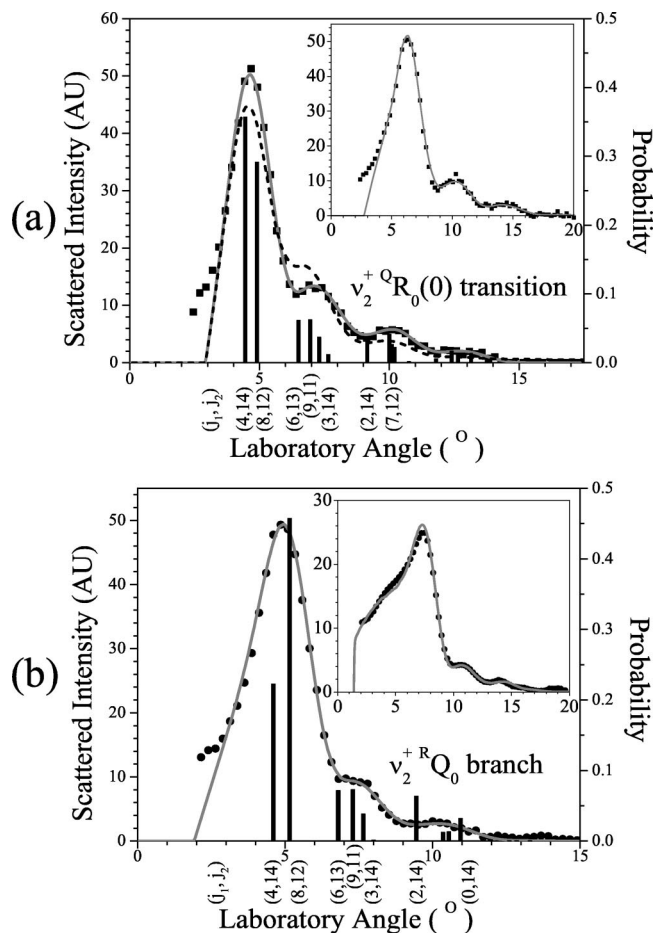

FIG. 6. Photofragment angular distributions for the ν_2^+ "bound" HCl stretch. In (a), the angular distributions associated with the $R(0)$ transition of the $K_a = 0 \leftarrow 0$ band and in (b) the (unresolved) $K_a = 1 \leftarrow 0$ Q branch. In both cases, the insets show the same angular distribution obtained under slower-molecular-beam-velocity conditions by argon seeding. The solid line through the data points is the result of a Monte Carlo calculation over all the experimental parameters. The quantum number assignment (j_1, j_2) for the most important channels is denoted under the vertical bars indicating the probability for each channel. The dashed line in (a) is the simulated theoretical angular distribution.

a recoil energy of 74 cm^{-1}. The additional structure in the angular distribution is associated with the other rotational channels in Fig. 7. Careful examination of the angular positions of the peaks in the experiment is consistent with a dissociation energy of 439 cm^{-1}. Unfortunately, as can be seen from Fig. 7, several open channels are rather closely spaced, including the first two open channels—namely, $(j_1, j_2) = (4, 14)$ and $(8, 12)$—limiting the accuracy with which the dissociation energy can be independently determined. In fact, we can fit all angular distributions (including those associated to excitation of the "bound" ν_2 HCl stretch) using D_0's between 434 and 448 cm^{-1}. In the analysis which follows we simply use the value determined by Ni *et al.*[28]

The next step is to fit the experimental angular distributions. For this purpose, we have developed a program that calculates the angular distribution for a specific channel by Monte Carlo averaging over the instrumental geometry. The results of these calculations were then used to fit the experimental angular distribution using a least-squares procedure,
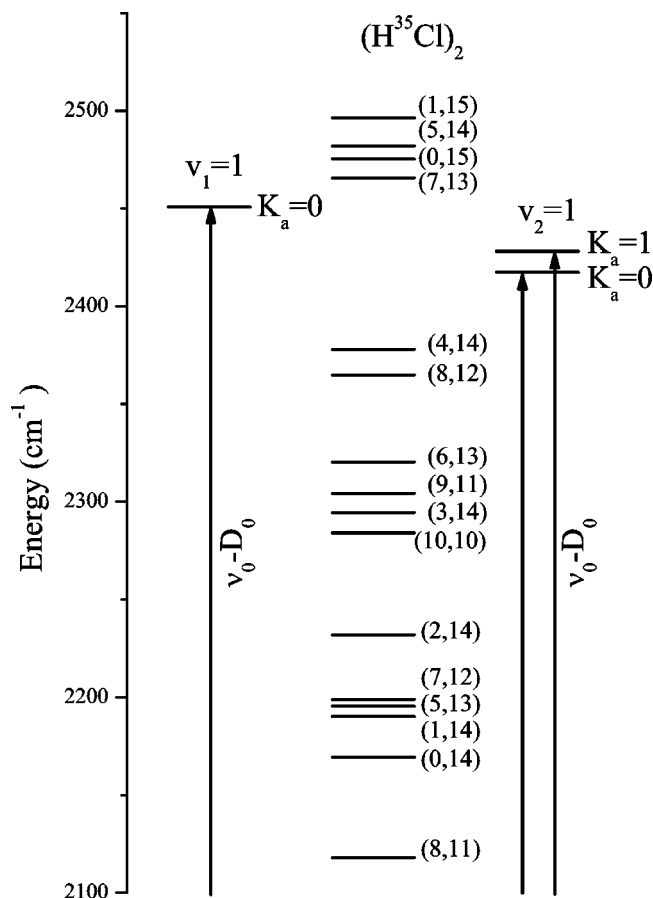
FIG. 7. Energy level scheme for the photodissociation of the H ^{35}Cl dimer. The vertical arrow shows the amount of energy available to the fragments following dissociation upon excitation of the "free" ν_1^+ (left arrow) or "bound" ν_2^+ HCl stretch (right arrows). Note that the first open channel is always $(j_1,j_2)=(4,14)$, independent of the specific vibrational excitation within the complex.

yielding the relative probabilities for the various photofragment channels. The solid line in Fig. 5 shows the result of this fitting procedure for the ν_1^+ $^R Q_0(1)$ transition and the vertical bars show the position of maximum intensity and the probability of the photofragment channels. The result of this fit is clearly in good agreement with the experimental results. The "argon-seeded" experimental angular distribution, shown as an inset of Fig. 5, was then calculated using the same probabilities, resulting in good agreement with experiment. This angular distribution establishes that there are no other photofragment channels at lower recoil energies, given that there are no additional peaks at angles smaller than 8.4°. As noted above, the anisotropy parameter β was set to zero in the Monte Carlo simulation. It is evident from Fig. 5 that the channel with the highest probability is the one with the lowest recoil energy: namely, $(j_1,j_2)=(4,14)$. In contrast, the next open channel (8,12) is much less probable even though it is only 13 cm^{-1} higher in recoil energy. It is important to note that the fitted probabilities are somewhat correlated, particularly for closely spaced channels.

We now turn our attention to the analysis of the experimental angular distributions for the ν_2^+ band. With the dissociation energy fixed at 439 cm^{-1}, Fig. 6 also shows the best fits for the ν_2^+ $^Q R_0(0)$- and $^R Q_0$-branch transitions.

Again, the vertical bars indicate the probabilities of the open photofragment channels. With the probabilities fixed, the "argon-seeded" angular distributions are also well reproduced. Note that the angular distributions for both ν_2^+ subbands are quite similar, as is the available energy. Apparently, the additional excitation of $K_a=1$ in the ν_2^+ HCl stretch does not significantly change the associated dissociation dynamics.

B. Comparison between calculations and experiments

The most direct way to compare the result of our calculations with the experimental data is to calculate the angular distributions that results from our computed rotational-state distributions. For the ν_2 state of B_2 symmetry, the result is shown in Fig. 6(a). The theoretical curve reproduces the experiment quite well, although the second peak is somewhat stronger in the calculation, reflective of the predicted probability for the (3,14) channel being somewhat too high. Given the sensitivity of the distribution to the potential surface, the agreement is actually surprisingly good. Unfortunately, we cannot compare the other experimental angular distributions in this way since they involve the additional excitation of $K=1$ in the vibrational excited state of the HCl dimer, for which no calculations were performed.

There have been three experimental studies by Ni and co-workers[28,43,45] on the rotational-state distribution of HCl fragments with which we can compare the results presented above. Using position-sensitive translational spectroscopy (POSTS),[43] they were able to determine a complete quantum-state-resolved distribution of rotational states $j_{HCl} \geq 10$. In Fig. 8(a) we show a comparison between their distributions[28] and those obtained from our theoretical and experimental data, by summing over the states of the other fragment: namely, $D(j_2)=\Sigma_{j1}P(j_1,j_2)$ for the ν_2 band. The $\pm$ labeling for IR transitions is used in this figure; i.e., the ν_2^+/ν_2^- transitions probe the upper/lower tunneling states of the dimer. It is clear that the probability distributions are qualitatively consistent with those of Ni and co-workers, although our experimental results suggest a somewhat larger contribution from the highest rotational state ($j_2=14$). Note that the agreement between the data of Ni and co-workers with our theoretical data is quite good for the ν_2^+ excitation. For the ν_2^- transitions the theoretical distributions underestimate the contributions from the $j_2=12$ and 13 states.

Figure 8(b) shows the distribution for dissociation from a ν_1 excited state. For the ν_1^-, the calculated probability for the highest rotational state ($j_2=14$) is clearly too large, while the theoretical distributions underestimate the contributions from the $j_2=12$ and 13 states. For the ν_1^+ excited state no direct comparison with experiments can be made, but looking at Fig. 8(b), we see that it closely resembles the experimental distribution of its tunneling partner, in fact more so than the calculation for this symmetry.

Ni and co-workers also determined the product correlation for states in which one of the molecules is in rotational state $j_2=14$,[43] indicating that a major fraction, 86%, was found in (4,14) and 14% in (3,14). The upper limits for the ratio of the remaining $(j_1,14)$ states were estimated to be less

FIG. 9. j_1, j_2 correlation plot for the ν_2 excited state of A_1 symmetry. The experimental data are from Ref. 28.

dissociation channels to the rotational-state distributions of the ν_2 excited state of A_1 symmetry. It is immediately obvious from Fig. 9 that the computed contributions to the (8,12) and (6,13) channels are much too low when compared with the experimental distribution of Ni *et al.*[28] The lack of probability in these two channels is the cause of the low probabilities for $j_2 = 12$ and 13 in Fig. 8(a). A further comparison with the experimental data for the ν_1 (Ref. 28) is not possible due to an apparent error in the plotting of their correlated probabilities.[61]

Fárník *et al.*[47,62] found two interesting trends for the combined excitation of a monomer stretch mode and the ν_4 and ν_5 excitations. The first was that all observed transitions were based on the excitation of the donor stretch ν_2 and the second that three of the four observed combination bands originated from the upper tunneling level of the ground state. Our full-dimensional calculations of the line strengths for transitions from the $J = 1$, $K = 0$ ground state to $J = 0$ predissociating states support both observations; see Table VI. The $\nu_2 + \nu_4$ and $\nu_2 + \nu_5$ transitions are much stronger than their ν_1 counterparts. Also, for these combined excitations, the transitions to the excited states of A_1 symmetry, which originate from the upper tunneling level of the ground state, clearly dominate.

This last effect is much stronger than in the case of HF dimer,[42] as was already pointed out by Fárník *et al.*[62] They explain this effect in terms of the fact that the tunneling barrier in $(HF)_2$ is much higher than in the HCl dimer. As a result, the HF dimer wave functions are much more localized in the two wells on the ν_5 tunneling path. The difference between A_1 and B_2 tunneling states is then much smaller than in HCl dimer, where the A_1 states have significant amplitude in the region of the barrier, whereas the B_2 states have a nodal plane in this location.

It is interesting to note that the strongest combination band, according to our calculations, is $(\nu_2 + \nu_5)^-$, which was also found to be strongest in the 3D model calculation by Fárník *et al.* Nevertheless, it was not observed in their experiments, although the computed energy difference (2897
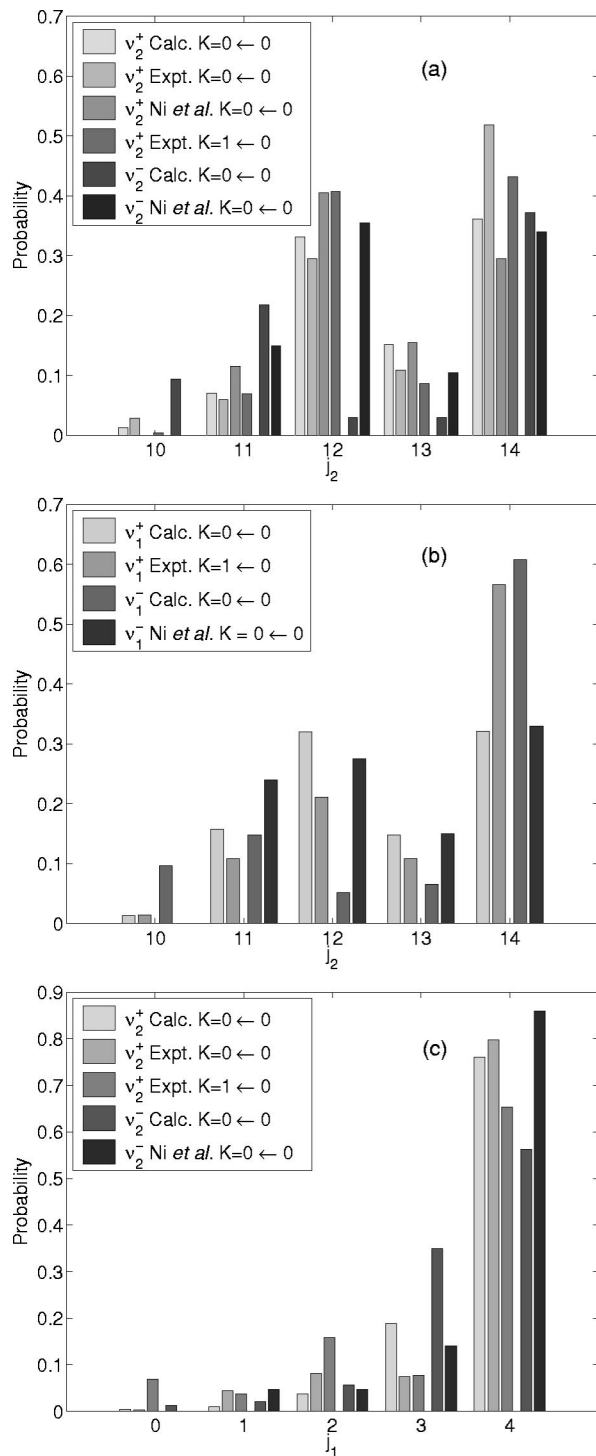

FIG. 8. Rotational-state distributions of the HCl fragments. Panels (a) and (b) show the distributions summed over j_1 for dissociation from ν_2 and ν_1 excited states, respectively. Panel (c) shows the distribution for $j_2 = 14$ for ν_2 excited states. The experimental data by Ni *et al.* are from Ref. 28.

than 5% for $j_1 = 2$ and less than 2% for $j_1 = 1$ with essentially no population of the (0,14) channel. Figure 8(c) shows a comparison of their results with the present experimental and theoretical data. Here again we see that the ν_2^+ distribution agrees better with the experimental data [see also Fig. 6(a)] than that of ν_2^-.

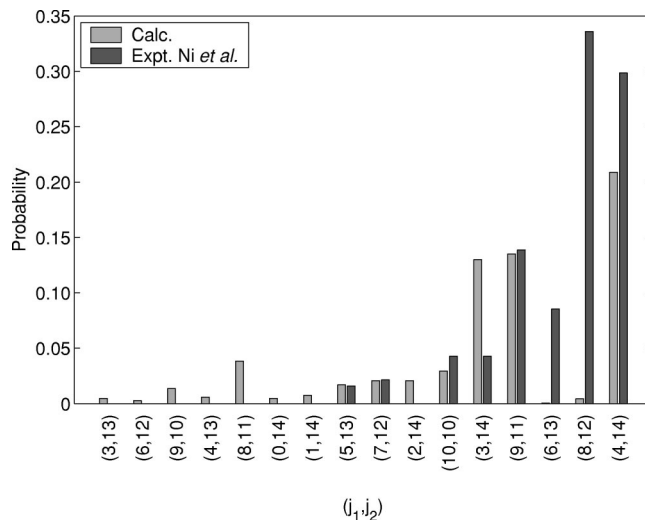Looking in more detail at the dissociation channels individually, we show in Fig. 9 the contributions of the highest

cm^{-1}) places it in the region of the spectrum that was investigated.

VII. COMPARISONS BETWEEN THE HCl AND HF DIMERS

In making comparisons between the photodissociation dynamics of HCl and HF dimers it is important to emphasize that the overall trend in the latter system was for the population of "high-j–low-j" exit channels, explained in terms of an impulsive dissociation from equilibrium geometry resulting in high/low rotational excitation of the proton donor/ acceptor fragments. In addition, states with low recoil energies were preferred over those with high translational energies. The experimental results for HCl dimer presented here are also highly nonstatistical, again showing preference for channels with low recoil energies. On the other hand, the similar probabilities for the (4,14) and (8,12) channels suggest a lack of clear "high-j–low-j" exit channels, as also illustrated by a low probability for other (j_1,14) channels. This is consistent with the floppier nature of the HCl dimer, which makes the asymmetric proton-donor/proton-acceptor geometry less important than for HF dimer.

VIII. CONCLUSION

We have studied the vibrational predissociation of HCl dimer using both theory and experiment. All of the experimental results presented here are consistent with the dissociation energy of 439 cm^{-1} reported by Ni *et al.*[28] Furthermore, we find that the polarization of the laser does not have an effect on the observed angular distributions, in contrast with earlier observations on the HF dimer. We attribute this effect to the nuclear hyperfine depolarization in the case of $(HCl)_2$.

Calculations based upon the ES1–EL potential energy surface give linewidths that are 1–2 orders of magnitude smaller than experiment. The rotational-state distributions agree reasonably well with experimental data, although the computed distributions for scattering states of even permutation symmetry are systematically further from the experimental results. Given that the distributions are converged with respect to the angular basis, we suspect that this is a problem with the potential energy surface. Since the lifetime depends upon the coupling between the intramolecular and intermolecular coordinates in the small-R region of the potential, the implication is that the coupling is too weak. As was mentioned previously, there is other evidence that this coupling is also too weak in the ES1 potential. The ES1–EL potential was corrected by adding an r_A, r_B-dependent dipole–dipole interaction term, which is inherently long range. Hence the disagreement between calculated and measured linewidths can most likely be attributed to the fact that this correction term is only an estimate of the coupling. On the other hand, the rotational-state distributions are more dependent on the anisotropy of the ground-state potential. The fact that the ES1 potential is fit to spectroscopic data that directly probes this anisotropy suggests that the relevant interactions are faithfully reproduced. As a result, the rotational-state distributions are in better agreement with the experimental data than the linewidths. In comparison with the dissociation dynamics of the HF dimer, we find that HCl "high-j–low-j" exit channels are less dominant in the angular photofragment distributions. This is consistent with the floppier HCl dimer structure, which makes the two HCl subunits less distinguishable than in the equilibrium proton-donor/proton-acceptor geometry.

[1] N. Ohashi and A. S. Pine, J. Chem. Phys. **81**, 73 (1984).
[2] A. S. Pine and B. J. Howard, J. Chem. Phys. **84**, 590 (1986).
[3] N. Moazzen-Ahmadi, A. R. W. McKellar, and J. W. C. Johns, Chem. Phys. Lett. **151**, 318 (1988).
[4] G. A. Blake and R. E. Bumgarner, J. Chem. Phys. **91**, 7300 (1989).
[5] N. Moazzen-Ahmadi, A. R. W. McKellar, and J. W. C. Johns, J. Mol. Spectrosc. **138**, 282 (1989).
[6] T. R. Dyke, B. J. Howard, and W. Klemperer, J. Chem. Phys. **56**, 2442 (1972).
[7] W. J. Lafferty, R. D. Suenram, and F. J. Lovas, J. Mol. Spectrosc. **123**, 434 (1987).
[8] K. von Puttkamer and M. Quack, Mol. Phys. **62**, 1047 (1987).
[9] M. D. Schuder, C. M. Lovejoy, D. D. Nelson, and D. J. Nesbitt, J. Chem. Phys. **91**, 4418 (1989).
[10] D. T. Anderson, S. Davis, and D. J. Nesbitt, J. Chem. Phys. **104**, 6225 (1996).
[11] S. C. Althorpe, D. C. Clary, and P. R. Bunker, Chem. Phys. Lett. **187**, 345 (1991).
[12] P. R. Bunker, V. C. Epa, P. Jensen, and A. Karpfen, J. Mol. Spectrosc. **146**, 200 (1991).
[13] M. J. Elrod and R. J. Saykally, J. Chem. Phys. **103**, 921 (1995).
[14] M. J. Elrod and R. J. Saykally, J. Chem. Phys. **103**, 933 (1995).
[15] Y. Qiu and Z. Bačić, J. Chem. Phys. **106**, 2158 (1997).
[16] Y. Qiu, J. Z. H. Zhang, and Z. Bačić, J. Chem. Phys. **108**, 4804 (1998).
[17] M. Mladenović and M. Lewerenz, Chem. Phys. Lett. **321**, 135 (2000).
[18] M. Quack and M. A. Suhm, J. Chem. Phys. **95**, 28 (1991).
[19] Y. Volobuev, W. C. Necoechea, and D. G. Truhlar, J. Phys. Chem. A **101**, 3045 (1997).
[20] Q. Wu, D. H. Zhang, and J. Z. H. Zhang, J. Chem. Phys. **103**, 2548 (1995).
[21] D. H. Zhang, Q. Wu, J. Z. H. Zhang, M. von Dirke, and Z. Bačić, J. Chem. Phys. **102**, 2315 (1995).
[22] W. Klopper, M. Quack, and M. A. Suhm, Mol. Phys. **94**, 105 (1998).
[23] A. Furlan, S. Wülfert, and S. Leutwyler, Chem. Phys. Lett. **153**, 291 (1988).
[24] G. A. Blake, K. L. Busarow, R. C. Cohen, K. B. Laughlin, Y. T. Lee, and R. J. Saykally, J. Chem. Phys. **89**, 6577 (1988).
[25] A. Karpfen, P. R. Bunker, and P. Jensen, Chem. Phys. **149**, 299 (1991).
[26] F. M. Tao and W. Klemperer, J. Chem. Phys. **103**, 950 (1995).
[27] P. Jensen, M. D. Marshall, P. R. Bunker, and A. Karpfen, Chem. Phys. Lett. **180**, 594 (1991).
[28] H. Ni, J. M. Serafin, and J. J. Valentini, J. Chem. Phys. **113**, 3055 (2000).
[29] E. J. Bohac, M. D. Marshall, and R. E. Miller, J. Chem. Phys. **96**, 6681 (1992).
[30] A. S. Pine and W. J. Lafferty, J. Chem. Phys. **78**, 2154 (1983).
[31] R. L. DeLeon and J. S. Muenter, J. Chem. Phys. **80**, 6092 (1984).
[32] Z. S. Huang, K. W. Jucks, and R. E. Miller, J. Chem. Phys. **85**, 3338 (1986).
[33] D. C. Dayton, K. W. Jucks, and R. E. Miller, J. Chem. Phys. **90**, 2631 (1989).
[34] A. S. Pine and G. T. Fraser, J. Chem. Phys. **89**, 6636 (1988).

[35] M. D. Marshall, E. J. Bohac, and R. E. Miller, J. Chem. Phys. **97**, 3307 (1992).
[36] E. J. Bohac and R. E. Miller, J. Chem. Phys. **99**, 1537 (1993).
[37] L. Oudejans and R. E. Miller, J. Phys. Chem. A **101**, 7582 (1997).
[38] N. Halberstadt, P. Brechignac, J. A. Beswick, and M. Shapiro, J. Chem. Phys. **84**, 170 (1986).
[39] D. H. Zhang and J. Z. H. Zhang, J. Chem. Phys. **98**, 5978 (1993).
[40] D. H. Zhang and J. Z. H. Zhang, J. Chem. Phys. **99**, 6624 (1993).
[41] M. von Dirke, Z. Bačić, D. H. Zhang, Q. Wu, and J. Z. H. Zhang, J. Chem. Phys. **102**, 4382 (1995).
[42] G. W. M. Vissers, G. C. Groenenboom, and A. van der Avoird, J. Chem. Phys. **119**, 286 (2003).
[43] H. Ni, J. M. Serafin, and J. J. Valentini, J. Chem. Phys. **104**, 2259 (1996).
[44] M. D. Schuder, C. M. Lovejoy, R. Lascola, and D. J. Nesbitt, J. Chem. Phys. **99**, 4346 (1993).
[45] J. Serafin, H. Ni, and J. J. Valentini, J. Chem. Phys. **100**, 2385 (1994).
[46] R. F. Meads, A. L. McIntosh, J. I. Arnó, C. L. Hartz, R. R. Luchese, and J. W. Bevan, J. Chem. Phys. **101**, 4593 (1994).
[47] M. Fárník, S. Davis, and D. J. Nesbitt, J. Chem. Phys. **116**, 6132 (2001).
[48] M. Fárník, S. Davis, and D. J. Nesbitt, J. Chem. Phys. **118**, 10 137 (2003).
[49] G. C. Groenenboom and D. T. Colbert, J. Chem. Phys. **99**, 9681 (1993).
[50] G. W. M. Vissers, G. C. Groenenboom, and A. van der Avoird, J. Chem. Phys. **119**, 277 (2003).
[51] M. S. Child, *Molecular Collision Theory* (Academic, New York, 1974).
[52] *Handbook of Mathematical Functions*, edited by M. Abramowitz and I. A. Stegun (National Bureau of Standards, Washington, D.C., 1964).
[53] B. R. Johnson, J. Chem. Phys. **67**, 4086 (1977).
[54] F. X. Gadéa, H. Berriche, O. Roncero, P. Villarreal, and G. D. Barrio, J. Chem. Phys. **107**, 10 515 (1997).
[55] M. Geleijns, A. van der Avoird, P. E. S. Wormer, and N. Halberstadt, J. Chem. Phys. **117**, 7562 (2002).
[56] R. J. Bemish, E. J. Bohac, M. Wu, and R. E. Miller, J. Chem. Phys. **101**, 9457 (1994).
[57] L. Oudejans and R. E. Miller, J. Phys. Chem. **99**, 13 670 (1995).
[58] E. W. Kaiser, J. Chem. Phys. **53**, 1686 (1970).
[59] F. C. De Lucia, P. Helminger, and W. Gordy, Phys. Rev. A **3**, 1849 (1971).
[60] G. T. Fraser and A. S. Pine, J. Chem. Phys. **91**, 637 (1989).
[61] J. J. Valentini (private communication).
[62] M. Fárník, S. Davis, and D. J. Nesbitt, Faraday Discuss. **118**, 63 (2001).